Fault Detection and Estimation of Fault Redundant Airspeed using Unscented Kalman Filter

S. Janakiraman   Master Student, Control and Simulation, TU-Delft, 2629HS, Delft, the Netherlands. satya-narayanan.j@gmail.com

S. Schopferer   Team Leader Safe Autonomy, DLR Institute of Flight Systems, Braunschweig, Germany. Simon.Schopferer@dlr.de

C.C. de Visser   Associate Professor, Control and Simulation, TU-Delft, Delft, the Netherlands. c.c.devisser@tudelft.nl

ABSTRACT

Reliable measurements on key air data parameters such as air speed, angle of attack, and angle of sideslip are essential for safe flight operations. Unfortunately, due to their direct exposure to a sometimes hostile environment, air-data sensors are sensitive to faults. In order to maintain reliable knowledge of the air speed after pitot tube faults, the Double Model Adaptive Estimation (DMAE) method is combined with an Unscented Kalman Filter (UKF) estimation routine that uses a kinematic model that incorporates the effects of the turbulence. The approach requires sensor data from the pitot tube, angle of attack vanes, angle of sideslip vanes, and attitude angles from the Inertial Navigation System (INS). For the kinematic equation the Inertial Measurement Unit (IMU) data (Accelerometer / Gyroscope) are used to perform the estimation. The proposed approach is validated with data generated by a high-fidelity (nonlinear) Citation-550 Simulator. Realistic fault modes are used in the validation, including combinations of total pressure port and static pressure port blockages. With this approach, airspeed fault detection is performed and a fault redundant airspeed is estimated. The Augmented Fault UKF is found to achieve an unbiased state estimation even in the presence of unknown disturbances.

Nomenclature

V - *True airspeed in m/s*

α - *Angle of attack in radians*

β - *Angle of side slip in radians*

ϕ - *Roll angle in radians*

θ - *Pitch angle in radians*

ψ - *Yaw angle in radians*

q_c : *Impact Pressure*

M : *Mach number*

P : *Static Pressure*

P_0 : *Static Sea Level Pressure (ISA)*

γ_k : *Innovation*

A_{x_m} - *Measured Acceleration x axis in m/s^2*

A_{y_m} - *Measured Acceleration y axis in m/s^2*

A_{z_m} - *Measured Acceleration z axis in m/s^2*

p_m - *Measured Roll rate in radians/s*

q_m - *Measured Pitch rate in radians/s*

r_m - *Measured Yaw rate in radians/s*

$RMSE$ − *represents the Root Mean Square Error.*

n − *is the number of data points*

y_i − *refers to the predicted values*

$\hat{y}_i$ − *represents the observed values.*

$C(k)$: *Covariance of error of output state estimation*

a_0 : *Sonic Speed at Sea Level ISA (661.47 kts | 340.29 m/s)*

1 Introduction

The loss of reliable airspeed measurements can be catastrophic for flight safety, especially in scenarios where the Pitot tube malfunctions. In the article *"Preparing for a Safe Return to the Skies"*, published by Airbus in June 2020, the increased risk of unreliable airspeed events after parking or storing an aircraft is demonstrated. 44 out of 55 reported cases of unreliable air speed at take-off are due to an obstruction of the Pitot tube. Obstructions may be caused by the presence of insects, water, sand, dirt, dust, or other foreign materials that can enter the Pitot tube if protective covers do not cover the aircraft when it is on the ground. To overcome this, current aircraft are fitted with multiple Pitot tubes (hardware redundancy). For particular designs that cannot accommodate hardware redundancy, reliable airspeed remains a problem. This study proposes the use of an Unscented Kalman Filter (UKF) within the Double Model Adaptive Estimation approach [12] to estimate the flight envelope protection parameters. These flight envelope protection parameters are the Euler angles and airspeed, the angle of attack, and the angle of side slip.

Air data system fault detection is an extensively researched topic; the Boeing commercial airplane group published the Fault Tolerant Air Data and Inertial Reference System (FT-ADIRS) tested on its 777 airliner [14]. To assess the performance of the FT-ADIRS, a unique approach was adopted. The flight-recorded sensor data were replayed through actual production units, mimicking real-life scenarios. By randomly introducing faults in a Monte Carlo fashion, the system's ability to detect and overcome sensor failures in real time was thoroughly tested. This process demonstrated the robustness of the system in terms of inertial navigation and air data functions, demonstrating its ability to identify and survive sensor faults effectively [14]. The FT-ADIRS consists of the Fault Tolerant Air Data and Inertial Reference Unit (FT-ADIRU), the Secondary Attitude and Air Data Reference Unit (SAARU), and six Air Data Modules (ADMs). This is considered to be the first commercial version of the sensor fault-tolerant air-data and inertial system. Since then, many academic studies have come up with methodologies to tackle this problem; they can be broadly classified as data based methods [4]&[5] model-based methods [12] [9]&[18] and knowledge based methods [20]&[1].

In Lu et al. in [13] a Multiple-Model Adaptive Estimation (MMAE) technique was proposed; To improve computational efficiency and implementation simplicity, the Double-Model Adaptive Estimation (DMAE) was proposed in [12] and applied to flight data with simulated faults in [11]. The principle of these approaches is that multiple filters are programmed with different fault conditions. By analyzing the innovation variances of the filter, the fault condition is isolated. The DMAE approach can detect bias faults using a kinematic model of the aircraft and a selective re-initialization routine. The kinematic model resolves the issue of model uncertainties, making the approach more robust to such uncertainties. However, in [11] more realistic faults in the airspeed sensor (Pitot tube), such as sample-and-hold faults and drift faults, were not considered.

The main contribution of this paper is a fault detection and identification technique together with a fault redundant airspeed estimator in the presence of external disturbances under realistic pitot sensor faults. To address the situation when the effects of faults and external disturbances are coupled, two filters are constructed within the DMAE framework; one sensitive to the sensor noise & biases and the other filter sensitive to added noise. Finally, the probabilities of the two filters are calculated; the higher probability indicates the closeness of the estimated data to the state estimation and not necessarily the measured airspeed; which enables the computation of a fault redundant airspeed.
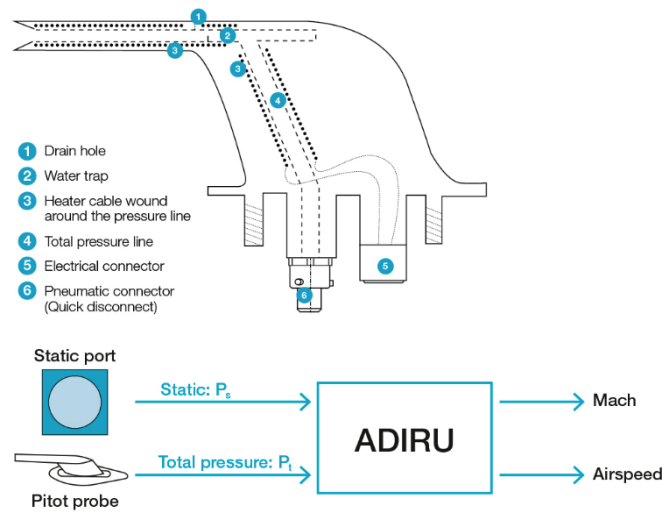
Fig. 1   Pitot tube layout [Source:Airbus]

2 Fault Scenario

A Pitot probe points directly into airflow, allowing it to measure the stagnation pressure known as the total pressure or Pitot pressure; see Fig. 1. When these total pressure data are combined with the static pressure, the Air Data Inertial Reference Unit (ADIRU) calculates the indicated airspeed and Mach number.

Table 1 details the fault modes considered in this paper. In case the total pressure port is completely obstructed, the airspeed indicator receives a relevant static pressure but a constant total pressure. Hence, the measured airspeed increases during climb and decreases during descent, and this can be simulated by including ramp faults to the measured airspeed for the fault detection simulation. In case all ports are blocked, no changes to the airspeed are reported, and this can be simulated by using a sample-and-hold signal to the measured airspeed. If only the static port is blocked, the measured airspeed decreases during climb and increases during descent, and this can again be simulated by the ramp fault signal.

3 Literature Review

Analytical redundancy provides two primary methods for determining the airspeed without using a Pitot probe. The first method utilizes information about the aircraft dynamic model to forecast airspeed based on control inputs. Although these methods are useful, they are limited to aircraft with an established and tested model, which may not always be available. This strategy employs dynamic model-aided navigation, including aerodynamic model parameters, in the navigation filter.

The second method for detecting airspeed without a Pitot probe involves using sensor fusion algorithms with other sensors. These methods have advantages over model-based approaches because they do not require a dynamic aircraft model. This method uses a kinematic model of the system based on multiple sensors, combining data from accelerometers, gyroscopes, Pitot probes, AOA/SSA vanes, and the global navigation satellite system (GNSS).

For the DLR-HAP case, a straightforward and reliable analytical redundancy-based Air Data Sensor Fault Detection (ADS-FD) method needs to be developed using data from onboard sensors and aircraft kinematics typically available for most current aircraft. To estimate air data, the proposed approach uses IMU measurements and onboard navigation system data (NSD), such as ground speed and Euler (attitude) angle data. This method does not take into account physical air data measurements, compared

Pitot-Static System Failure Modes

Failure	Altimeter Indicator Effect	Airspeed Indicator Effect	VSI Effect
Total Pressure port blocked	Not affected	Acts as an altimeter increases during climb decreasing during descent	Not affected
One static source blocked assuming two Sources	Inaccurate while slipping and skidding	Inaccurate while slipping and skidding	Inaccurate while slipping and skidding
Both static sources or single source blocked	Does not change with altitude; if blocked before take off, indicates field elevation	Decreases during climb and increasing during descent	Indicates the last vertical speed before blockage
All static and total pressure sources blocked	Indication remains constant regardless of actual change	Indication remains constant regardless of actual change	Indication remains constant regardless of actual change

Table 1   Fault Scenarios

with the usual air data estimates using redundant ADS. The main benefit of the approach followed by Lu et al. [12] is its applicability to any aircraft, without considering a specific aircraft model. Focuses only on sensor dynamics, ignoring system dynamics, and employs the aircraft equations of motion to create a streamlined mathematical model considering only the aircraft's own aerodynamic forces (X, Y, Z) and moments (L, M, N). This approach eliminates model mismatches and reduces tuning complexity. The state equation is determined by treating airspeed, angle-of-attack, sideslip angle, attitude angles, and wind velocity as a state vector, with attitude angle estimation being crucial for accurate and reliable air data estimation.

Numerous strategies for sensor fault detection have been proposed in recent decades. Miljković [15] reviewed several new Fault Detection and Isolation (FDI) techniques, discussing the latest developments in detail. Youn et al. [18] introduced an innovative dynamic model-based estimate for a UAV's attitude, 3-D wind, AOA, and SSA. Their proposed algorithm includes 3-D wind states as random walk processes. Balzano et al. [1] suggested creating and tuning FD schemes for true airspeed, angle-of-attack, and angle-of-sideslip sensors using data alone.

Aircraft pitot-static probes are necessary for accurate readings of airspeed and altitude and for safe flying. Traditionally, measurement integrity is achieved through a voting system and redundant sensor hardware, which incurs payload and expense penalties. Freeman, Seiler, and Balas [6] explored an analytical substitute for hardware redundancy using a mathematical model of defective and working pitot-static probes. They modeled common probe flaws, such as debris, ice, or water obstructions, using experimental wind tunnel data and physical air data linkages. These models were combined with a linear model of the NASA GTM (Generic Transport Model) aircraft under one flight state to create reliable defect detection filters. Johansen et al. [8] estimated the wind velocity, AOA, and SSA using only kinematic relationships, avoiding the need for aerodynamic models or other aircraft parameters. This method requires a sensor suite consisting of GNSS, IMU, and a pitot-static tube as a minimum configuration, assuming slowly varying winds. However, Johansen et al. could not validate the accuracy of the estimates because of the lack of direct measurements of alpha and beta.

Hansen and Blanke [7] proposed a diagnostic configuration using the ground speed from an onboard GPS device and typical UAV sensor values with a straightforward thrust model. They calculated residuals by obtaining two additional airspeed estimates. Including the ground speed vector allowed for an estimate for wind speed and direction. Using thrust-speed curves and a nonlinear adaptive observer to estimate engine thrust, the second airspeed estimate was calculated. They detected faults in airspeed sensors in UAVs using a statistical variation of the three separate residual signals. The data-driven air data sensor FDI approach's main benefits include being model-free and highly robust. Fravolini et al. [4] proposed a semi-automated data-driven approach for designing and tuning a complete FD scheme for the TAS sensor of aircraft, which requires high-quality data to effectively evaluate the fault detection algorithm.

Recently, using data from the Global Positioning System (GPS) and the Inertial Measurement Unit (IMU), Rhudy et al. [16] presented synthetic air data estimates to provide analytic redundant air data. Some studies, such as those of Cho et al. [3], proposed estimating airflow angle and wind speed using an integrated Extended Kalman Filter (EKF) and Inertial Navigation System and GPS information. These methodologies show that air data estimation and ADS fault detection are challenging when physical air data sensor measurements are not considered. However, they offer solutions to problems faced by previously installed external air data probes. Nonlinear estimators are preferred over other methods because the estimation technique significantly impacts the performance of the FDI methodology. Youn et al. [19] proposed estimating air data using information from flight control and navigation systems, demonstrating the feasibility of using onboard INS/GPS navigation system data for air data parameter estimation instead of traditional air data probe-based observations. However, this strategy works better for specific aircraft with precise dynamic models and is susceptible to environmental perturbations. Additionally, if system non-linearity increases, the typical EKF performance deteriorates, impeding estimation accuracy. Some researchers, such as Lu [10], have suggested analytical techniques for identifying aviation sensor faults based on the EKF, which require intricate computations, potentially lengthening the computation times, then Lu et al. [11] introduced a double model adaptive estimation (DMAE) technique that saves computation times.

4 Kinematic Model

The kinematic model presented in Van Eykeren and Chu[17] is based on specific measured forces, allowing us to avoid calculations involving uncertain aerodynamic parameters. This model remains valid throughout the entire range of flight conditions, eliminating the need to design a limited parameter variable (LPV) system. Lu et al. [11] tested the kinematics with unknown external disturbances such as turbulence. The process model is of the form given in equation 1:

$$\dot{x} = \bar{f}(x, u) + G(x)w \tag{1}$$

Where

$$x = \begin{bmatrix} V & \alpha & \beta & \phi & \theta & \psi \end{bmatrix}^T \tag{2}$$

These are the measured & estimated states, the kinematics are based on the fact that these states are correlated to acceleration and turn rates. u is the input vector given in equation 3 which form the basis of airspeed computation.

$$u = \begin{bmatrix} A_{x_m} & A_{y_m} & A_{z_m} & p_m & q_m & r_m \end{bmatrix}^T \tag{3}$$

Accelerations on the 3 axis from the accelerometers and turn rates from the gyroscopes are used in estimating the states. The nonlinear function $\bar{f}$ is as follows:

$$\bar{f}(x,u) = \begin{array}{l} (A_{xm} - gs\theta)\,c\alpha c\beta + (A_{ym} + gs\phi c\theta)\,s\beta \\ \quad + (A_{zm} + gc\phi c\theta)\,s\alpha c\beta \\ [(A_{zm} + gc\phi c\theta)\,c\alpha - (A_{xm} - gs\theta)\,s\alpha]\,/Vc\beta + q_m \\ \quad - (p_m c\alpha + r_m s\alpha)\,t\beta \\ [(gs\theta - A_{xm})\,c\alpha s\beta + (A_{ym} + gs\phi c\theta)\,c\beta \\ \quad - (A_{zm} + gc\phi c\theta)\,s\alpha s\beta]\,/V + p_m s\alpha - r_m c\alpha \\ p_m + q_m s\phi t\theta + r_m c\phi t\theta \\ q_m c\phi - r_m s\phi \\ q_m s\phi/c\theta + r_m c\phi/c\theta \end{array}$$

In the implementation of this non-linear function, the Euler method of time discretization is used. Here, $c\alpha$ refers to $\cos(\alpha)$, $s\beta$ is $\sin(\beta)$ and so on. The IMU input noise distribution matrices $G(x)$ are derived as follows:

$$G(x) = \begin{bmatrix} -c\alpha c\beta & -s\beta & -s\alpha c\beta & 0 & 0 & 0 \\ \frac{s\alpha}{Vc\beta} & 0 & \frac{-c\alpha}{Vc\beta} & c\alpha t\beta & -1 & s\alpha t\beta \\ \frac{c\alpha s\beta}{V} & \frac{-c\beta}{V} & \frac{s\alpha s\beta}{V} & -s\alpha & 0 & c\alpha \\ 0 & 0 & 0 & -1 & -s\phi t\theta & -c\phi t\theta \\ 0 & 0 & 0 & 0 & -c\phi & s\phi \\ 0 & 0 & 0 & 0 & \frac{-s\phi}{c\theta} & \frac{-c\phi}{c\theta} \end{bmatrix}$$

where $w = \begin{bmatrix} w_{A_x} & w_{A_y} & w_{A_z} & w_p & w_q & w_r \end{bmatrix}^T$ denotes the noise in the inertial measurement unit.

5 Methodology

The Unscented Transform (UT) is well suited for state estimation in the framework of a nonlinear time-varying aircraft model. The UT calculates statistics of a random variable after a nonlinear transformation. The UT approximates a Gaussian distribution, which is more straightforward than approximating an arbitrary nonlinear function. The Extended Kalman Filter (EKF) approximates a nonlinear function using linearization. However, this can be insufficient when models have significant non-linearities over short time periods. The work of Caveney[2] illustrates that the combination of UT and numerical integration can provide significantly more accurate stochastic predictions of the future state of a nonlinear system at lower computational cost than similar Kalman-like routines.

To address the issue that sensor noise, biases and fault conditions cannot be differentiated from each other, this paper proposes a two-UKF filter approach where one filter assumes additive noise, from here refered to as the "Augmented Fault Filter (AF)" and the other filter assumes non-additive noise with a noise distribution matrix G(x) refered to as the "Sensor Noise and Bias Filter (SNBF)". The logic behind this being that when no fault is detected, the SNBF estimate would be closest to the ground truth, and when a fault is detected, the AF filter estimate is closest to the ground truth. The AF filter is used to create a fault redundant estimate of the states. Modal probabilities are used as a fault detection metric.

For aircraft ADS FDD, we still need to formulate the state transition model, measurement model, fault identification logic, and construct the UKF filters which in our case are of standard design.

Given below are an extract of the unscented transform methodology that the filter executes for each time step:

1) Introduction
   - The UKF extends the Kalman Filter for accurate estimation in nonlinear systems.
   - Sigma-Point Transformation is a key step in the UKF process.
2) Sigma-Point Selection
   - Deterministic approach (Unscented Transform) for sigma point selection.
   - Sigma points chosen symmetrically around the mean.
   - The number of sigma points depends on the state-space dimension.
3) Augmentation
   - Augment state vector and covariance matrix for additional process/measurement noise.
   - Augment the additional state - estimated fault state.
4) Propagation Through Nonlinear Functions
   - Apply process model function $f(x, u)$ to sigma points to predict new state points.
   - For each sigma point i, compute the predicted state $x_{k|k-1}^{(i)}$.
5) Estimation of Mean and Covariance
   - Compute weighted mean and covariance of predicted sigma points.
   - Weighted mean:

$$\bar{x}_{k|k-1} = \sum_{i=0}^{2n} W_m^{(0)} \cdot x_{k|k-1}^{(i)}$$

   - Weighted covariance:

$$\bar{P}_{k|k-1} = \sum_{i=0}^{2n} W_c^{(0)} \cdot (x_{k|k-1}^{(i)} - \bar{x}_{k|k-1})(x_{k|k-1}^{(i)} - \bar{x}_{k|k-1})^T + Q_k$$

6) Predict Measurements
   - Use predicted state to compute predicted measurements through function h().
7) Update Weights(Wc & Wm) and Cross-Covariance
   - Compute weights for transformed sigma points.
   - Compute the cross-covariance matrix between the original state and the predicted state.
   - Update state estimate and covariance using standard Kalman Filter equations.
   - Incorporate actual measurements for better estimation.
8) Advantages of UKF
   - Accurate estimation in nonlinear systems.
   - Captures nonlinear relationships between state and measurements.
9) Conclusions
   - Sigma-Point Transformation is a vital step in the UKF algorithm.
   - Enables more accurate state estimation in nonlinear scenarios.

5.1 State Transition UKF Model Architecture ($\dot{x}$)

f_V is the Augmented airspeed fault state, the state vector of the AF filter is x_{af} and the SNBF is x_{SNBF}

$$x_{af} = \begin{bmatrix} V & \alpha & \beta & \phi & \theta & \psi & f_V \end{bmatrix}^T \qquad x_{SNBF} = \begin{bmatrix} V & \alpha & \beta & \phi & \theta & \psi \end{bmatrix}^T$$

By augmenting f_V in the state transition model as an additional zero mean state, the Unscented Kalman filter estimates the fault in the first state, that is, the true airspeed state V. Similarly, this can be scaled to estimate all six states fault.

5.2 Measurement Function UKF Architecture (y)

Care is taken so that the AF and SNBF filters use the same measurement history vector y_k given in equation 6 and input vector u_k as defined in equation 3. The mapping to the estimated state parameters and the measurement vectors differ according to $y_k = H * X$. The mapping of f_v as an additive fault and programming the AF filter with additive noise enables the filter to estimate the fault.

$$y_k = \begin{bmatrix} V_m & \alpha_m & \beta_m & \phi_m & \theta_m & \psi_m \end{bmatrix}^T \tag{6}$$

The measurement model for augmented fault filter is Y_{af}

$$Y_{af} = \begin{bmatrix} V_m \\ \alpha_m \\ \beta_m \\ \phi_m \\ \theta_m \\ \psi_m \end{bmatrix} = \begin{bmatrix} 1 & 0 & 0 & 0 & 0 & 0 & 1 \\ 0 & 1 & 0 & 0 & 0 & 0 & 0 \\ 0 & 0 & 1 & 0 & 0 & 0 & 0 \\ 0 & 0 & 0 & 1 & 0 & 0 & 0 \\ 0 & 0 & 0 & 0 & 1 & 0 & 0 \\ 0 & 0 & 0 & 0 & 0 & 1 & 0 \end{bmatrix} \times \begin{bmatrix} V \\ \alpha \\ \beta \\ \phi \\ \theta \\ \psi \\ f_v \end{bmatrix} \tag{7}$$

The measurement model for sensor noise and bias filter is Y_{SNBF}

$$Y_{SNBF} = \begin{bmatrix} V_m \\ \alpha_m \\ \beta_m \\ \phi_m \\ \theta_m \\ \psi_m \end{bmatrix} = \begin{bmatrix} 1 & 0 & 0 & 0 & 0 & 0 \\ 0 & 1 & 0 & 0 & 0 & 0 \\ 0 & 0 & 1 & 0 & 0 & 0 \\ 0 & 0 & 0 & 1 & 0 & 0 \\ 0 & 0 & 0 & 0 & 1 & 0 \\ 0 & 0 & 0 & 0 & 0 & 1 \end{bmatrix} \times \begin{bmatrix} V \\ \alpha \\ \beta \\ \phi \\ \theta \\ \psi \end{bmatrix} \tag{8}$$

5.3 Fault Introduction/Identification

To simulate the airspeed fault scenario where the total pressure port and static pressure port are blocked, faults are introduced in the dynamic pressure and static pressure calculations. The reason for choosing this approach is because static pressure can be extracted from the equivalent airspeed measurement, and dynamic pressure can be extracted from the true airspeed measurement. The altitude information is required to interpret the temperature using the Committee on Extension to the Standard Atmosphere (COESA) Atmosphere Model. The temperature information is used to calculate the speed of sound, which in turn is required to calculate the Mach number:

$$M = \sqrt{5\left[\left(\frac{q_c}{P} + 1\right)^{2/7} - 1\right]} \qquad\qquad EAS = a_0 M \sqrt{\frac{P}{P_0}} \tag{9}$$

The ramp, step, pulses, and sample & hold faults are introduced into the time signal in the simulation, and the filter receives only the faulty airspeed measurement as described in Table 1. The faults are identified by comparing both filter innovation γ_k and output state estimation error covariance C_k (AF & SNBF) as

in [12]. The faults are estimated by adding an additional state (i.e. f_V) to the augmented fault filter. The output error covariance matrices of both the filters are given in equation 10, C_{AF} & C_{SNBF} are:

$$C_{SNBF} = \begin{bmatrix} C_{V,V} & C_{V,\alpha} & C_{V,\beta} & C_{V,\phi} & C_{V,\theta} & C_{V,\psi} \\ C_{\alpha,V} & C_{\alpha,\alpha} & C_{\alpha,\beta} & C_{\alpha,\phi} & C_{\alpha,\theta} & C_{\alpha,\psi} \\ C_{\beta,V} & C_{\beta,\alpha} & C_{\beta,\beta} & C_{\beta,\phi} & C_{\beta,\theta} & C_{\beta,\psi} \\ C_{\phi,V} & C_{\phi,\alpha} & C_{\phi,\beta} & C_{\phi,\phi} & C_{\phi,\theta} & C_{\phi,\psi} \\ C_{\theta,V} & C_{\theta,\alpha} & C_{\theta,\beta} & C_{\theta,\phi} & C_{\theta,\theta} & C_{\theta,\psi} \\ C_{\psi,V} & C_{\psi,\alpha} & C_{\psi,\beta} & C_{\psi,\phi} & C_{\psi,\theta} & C_{\psi,\psi} \end{bmatrix} \quad C_{AF} = \begin{bmatrix} C_{V,V} & C_{V,\alpha} & C_{V,\beta} & C_{V,\phi} & C_{V,\theta} & C_{V,\psi} & C_{V,fv} \\ C_{\alpha,V} & C_{\alpha,\alpha} & C_{\alpha,\beta} & C_{\alpha,\phi} & C_{\alpha,\theta} & C_{\alpha,\psi} & C_{\alpha,fv} \\ C_{\beta,V} & C_{\beta,\alpha} & C_{\beta,\beta} & C_{\beta,\phi} & C_{\beta,\theta} & C_{\beta,\psi} & C_{\beta,fv} \\ C_{\phi,V} & C_{\phi,\alpha} & C_{\phi,\beta} & C_{\phi,\phi} & C_{\phi,\theta} & C_{\phi,\psi} & C_{\phi,fv} \\ C_{\theta,V} & C_{\theta,\alpha} & C_{\theta,\beta} & C_{\theta,\phi} & C_{\theta,\theta} & C_{\theta,\psi} & C_{\theta,fv} \\ C_{\psi,V} & C_{\psi,\alpha} & C_{\psi,\beta} & C_{\psi,\phi} & C_{\psi,\theta} & C_{\psi,\psi} & C_{\psi,fv} \\ C_{fv,V} & C_{fv,\alpha} & C_{fv,\beta} & C_{fv,\phi} & C_{fv,\theta} & C_{fv,\psi} & C_{fv,fv} \end{bmatrix} \tag{10}$$

Innovation γ_k is defined as the difference between the measurement data and the estimated data. f_{y_k} given in equation 11 is the probability density function in Gaussian form given by:

$$f_{y(k)} = \beta(k) \exp\left\{-\gamma^T(k)C^{-1}(k)\gamma(k)/2\right\} \tag{11}$$

$$\beta(k) = \frac{1}{(2\pi)^{m/2}|C(k)|^{1/2}} \tag{12}$$

With the probability density function, the probability of the two filters are computed and denoted as $p_i(k)$, $i = 1, 2$.

1 - Augmented fault filter & 2 - Sensor noise and bias filter.

These probabilities are calculated at every time step k. As the fault occurs, innovation increases for the augmented fault filter, while the sensor noise & bias filter will follow the measurement signal, leading to low innovation. This difference in innovation can signify that a fault has occurred. The probabilities are computed as follows:

$$p_i(k) = \frac{f_{y_{ki}}p_i(k-1)}{\sum_{i=1}^{2} f_{y_{ki}}p_i(k-1)} \tag{13}$$

Using (13), the probability of the AF filter is 1 when the data have the highest correlation with a fault being present, while the probability of the SNBF filter is 0. In contrast, when no fault is detected, the probability of the SNBF filter is 1 and the AF filter is 0.

The redundant fault airspeed is obtained by following this probability distribution to select between the AF and SNBF filter estimates. In cases where the probability calculation fails, another redundant fault detection metric is used. This metric is based on the estimated fault when the filter is initialized. In this case, we take the 50 time step and 100 time step estimated fault values, then average this value and by considering a 40% margin the detection limit of the fault detection routine is set. When the AF filter estimates a fault greater than this detection limit, a fault is assumed to have occurred.

Based on the fault scenario that occurs in the Pitot tube and on the signal characteristics of those faults, the test scenarios are set according to Table 2.

Figure 2 represents the characteristics of the sample-and-hold fault. Sample and hold faults are particularly challenging to identify, as the fault effect may be relatively small for constant and slowly changing ADS measurements, and thus may stay 'hidden' for longer periods before becoming noticeable.
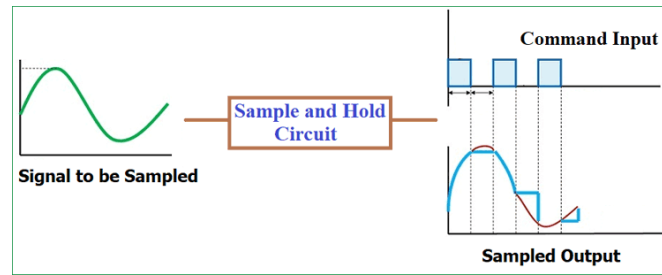
**Fig. 2   Sample and hold signal for fault introduction**

Table 2   Test cases for simulation

| Test Data	Fault vector	Test Scenario
		Pitot tube
(Simulation Data)	Ramp	Partially blocked ports
Cessna Citation 550 Simulation	Pulse generator	Fluttering particles in the ports
	Step	Simple Fault
	Sample and hold	Fully blocked ports

6 Results

In this section, the ADS FDD system is tested on data from a high-fidelity Cessna Citation 550 simulation. Figure 3 details the simulation setup, the simulation is divided into 4 sections: 1) Measured Flight Data Block - This block has the Pitot tube sensor emulation and fault introduction procedure. 2) Augmented fault filter - UKF with augmented fault state and the state transition function & the measurement function. 3) Sensor Noise and Bias Filter block UKF with nonadditive noise. 4) Fault estimation, prediction, and correction block - the probability calculation, and fault indicator. The 4th block will estimate the redundant airspeed from the fault.

Data from a 600-second run with the Cessna Citation 550 model are presented in Figure 10. As can be seen in Figure 6 the true air speed is constant at 90 m/s to 100 seconds during which the aircraft is flying level 10. At 100 seconds, an aileron pulse input causes the aircraft to transition into the spiral mode; at 200 seconds the elevator pulse input causes the aircraft to lose altitude; at 300 seconds a rudder pulse input causes the spiral mode to tighten. These inputs cause a sharp spike in the IMU measurements (Acceleration/turn rates); how the algorithm performs during these spikes in the input will be key in validating the functioning of the ADS FDD. The UKF relies on these input accelerations and turn rates to estimate the measurement states. The total flight time is 600 seconds, which is significantly longer than normally presented in the literature (see e.g. [10] and [12]). Our FDD algorithm is also tested with band-limited white noise added to the measurement vector, and the filter does not have a priori knowledge of the statistics of this noise. Table 3 gives the summary of the results without measurement noise.
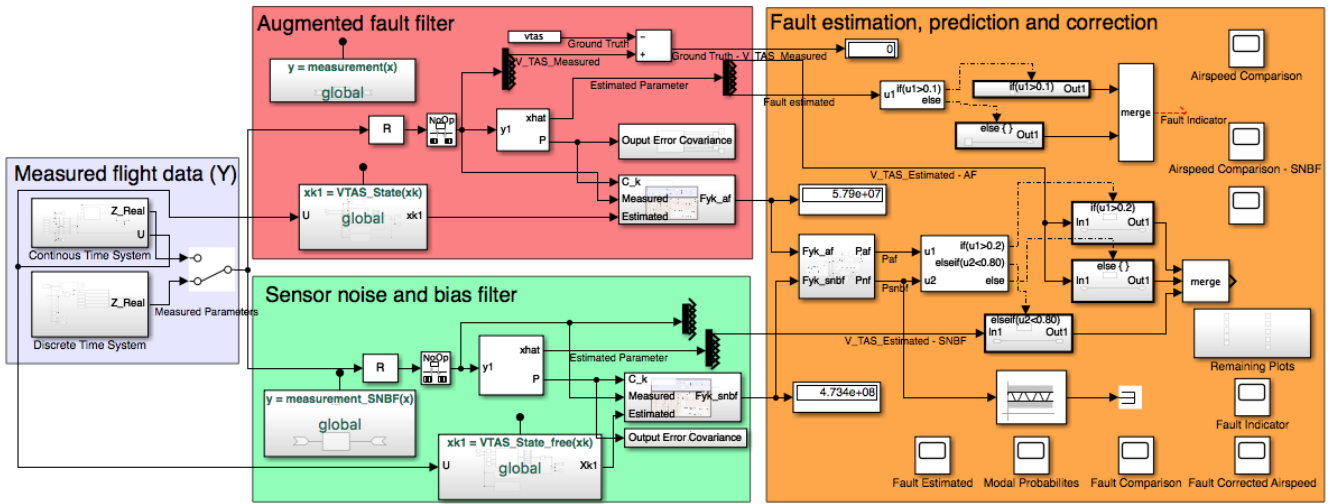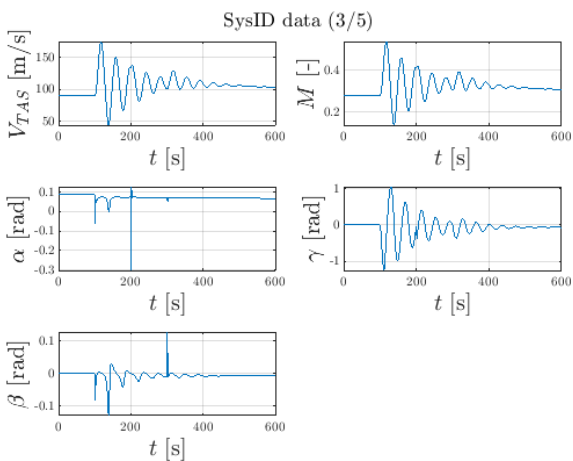
Fig. 3 ADS FDD and redundant airspeed estimation simulink implementation
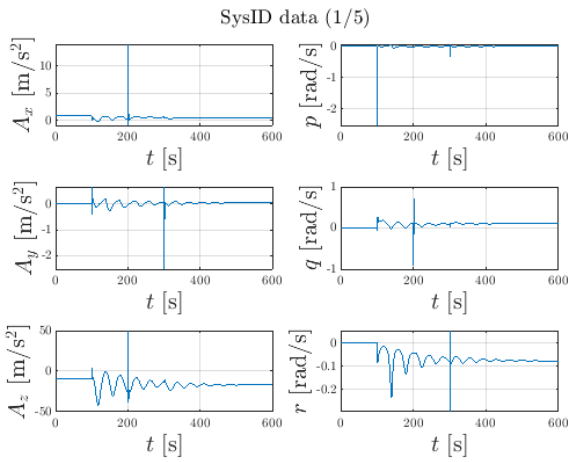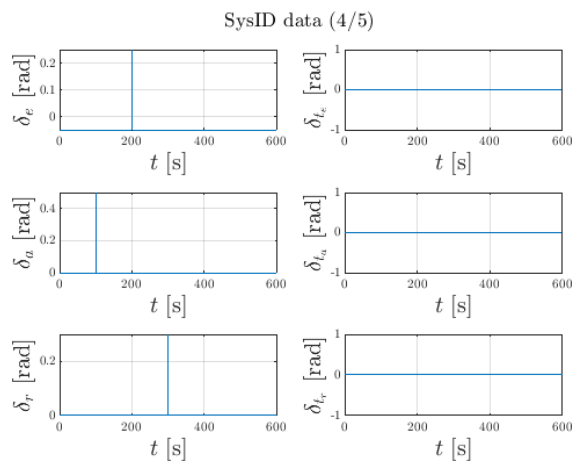

Fig. 4 Inertial Measurement unit data - U
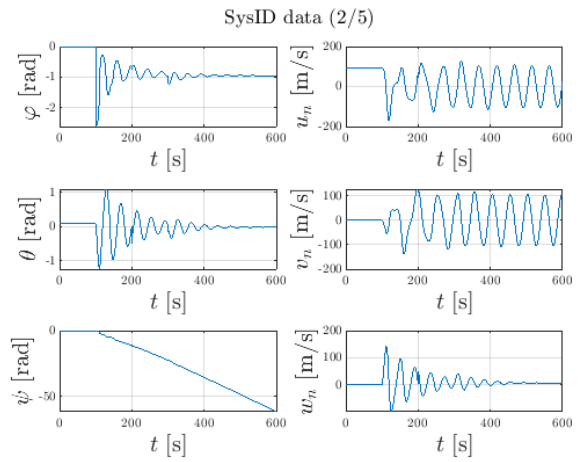
Fig. 5 Flight path angles

Fig. 6 True airspeed, angle of attack, angle of sideslip and mach number


Fig. 7 Control surfaces excitation

Cessna Citation Simulator data - 100 sec. Flight Data with aileron pulse input, 200 sec. elevator pulse input and 300 s. rudder pulse input.

6.1 Results of the FDD algorithm without noise

This subsection evaluates the performance of the FDD algorithm in an ideal scenario without measurement noise. As seen in Table 3 four test cases with faults induced by the sample and hold, step, ramp, and pulse generator are examined. The efficacy of the algorithm is depicted through:

1) Probability of Correct Filter Selection: Indicating the algorithm's ability to select the appropriate filter in a noise-free environment.
2) Fault Estimation by an AF Filter: Assessing the fault estimation capabilities of the AF filter without interference from measurement noise.
3) Corrected air speed: Demonstrating the algorithm's success in correcting airspeed under fault conditions.
4) Airspeed Comparison with Ground Truth: Ensure the reliability of the corrected airspeed in the absence of noise.

Figure 8 presents the results with pulse generator faults representing fluttering particles in the pitot tube. Another motivation to test this kind of fault is to test whether the algorithm can detect simple faults (step faults) during maneuvers. The probability plots and correct fault estimation show that the FDD is working as intended.
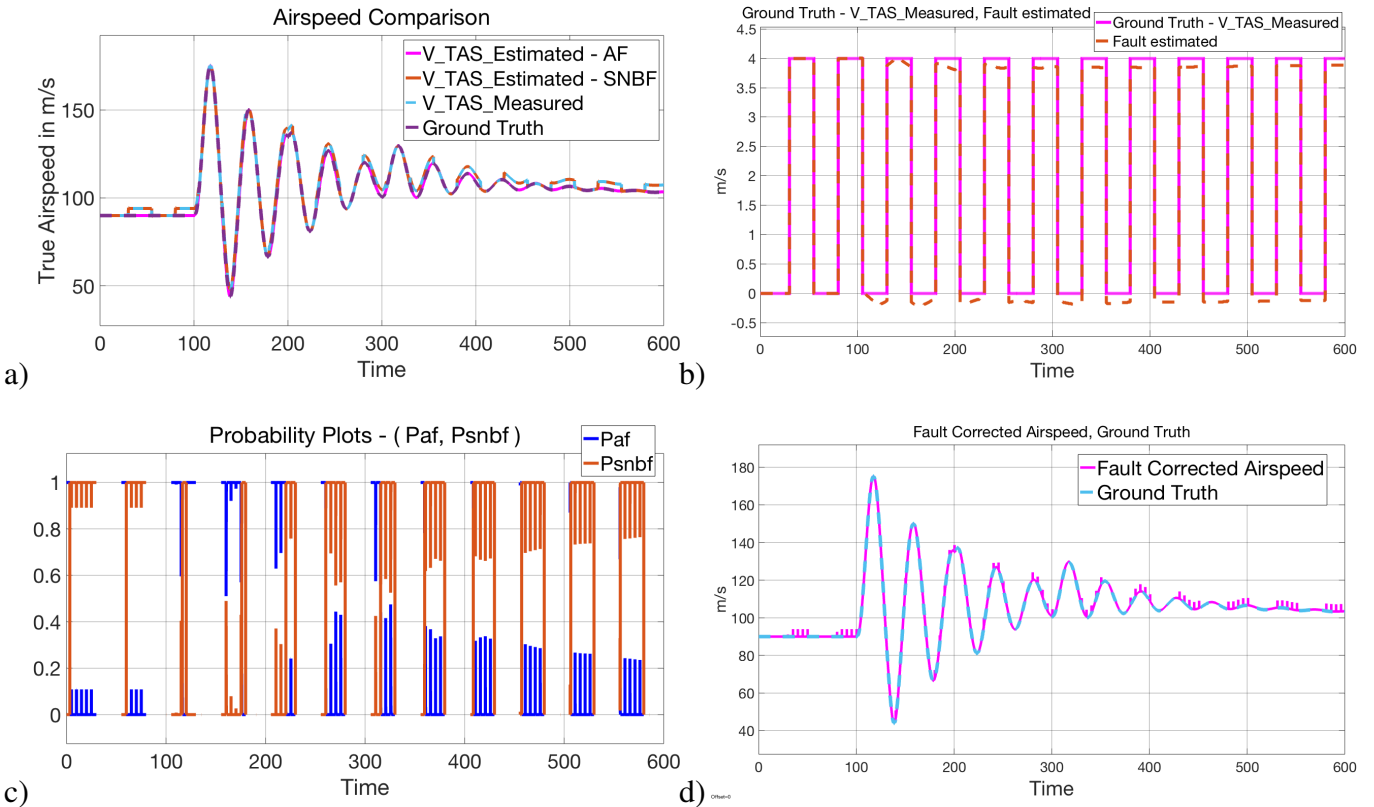

Fig. 8   ADS FDD performance to simulation with pulse generator fault. a) The airspeed comparison plot presents the airspeed data generated by both filters (SNBF & AF filter), alongside the fault-introduced airspeed and the ground truth airspeed. b) The plot represents the fault estimated by Augmented fault filter vs fault introduced in the system. c) Represents the probability of the both the filters. d) Corrected Airspeed generated by augmented fault filter vs ground speed.

Figure 9 shows the test plots with a simple step fault introduced at 100 seconds. It can be seen from the probability graph that the sensor noise and bias filter probability is higher when the filter detects no fault. When the filter detects the fault, the augmented fault filter has a higher probability. These probabilities change at 100 seconds; this is an indicator that there is no noise present in the system. Clearly, the FDD system can identify the fault in this noise-free situation. The estimated fault by the augmented fault filter has a magnitude of approximately 2 m/s at 100 s, which correctly corresponds to the step fault inserted into the measurement signal.
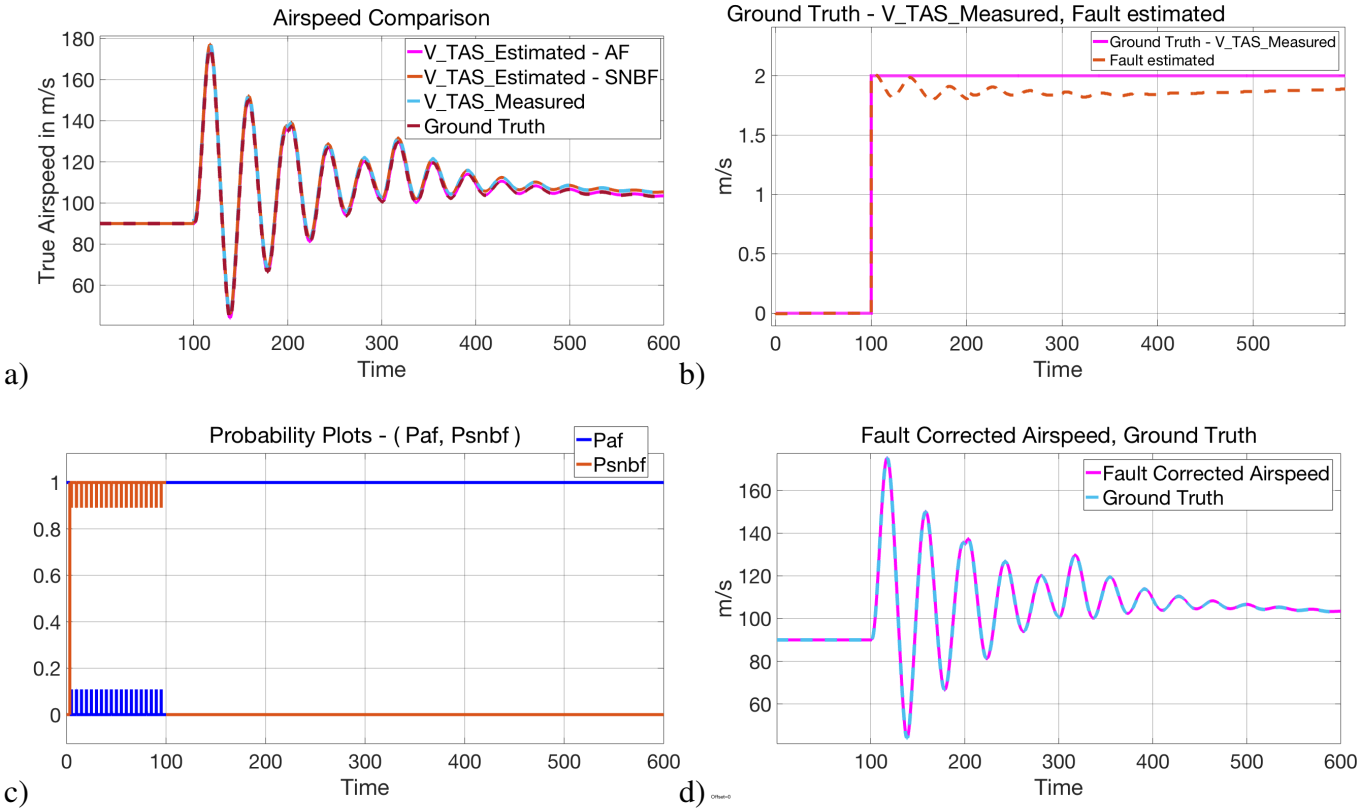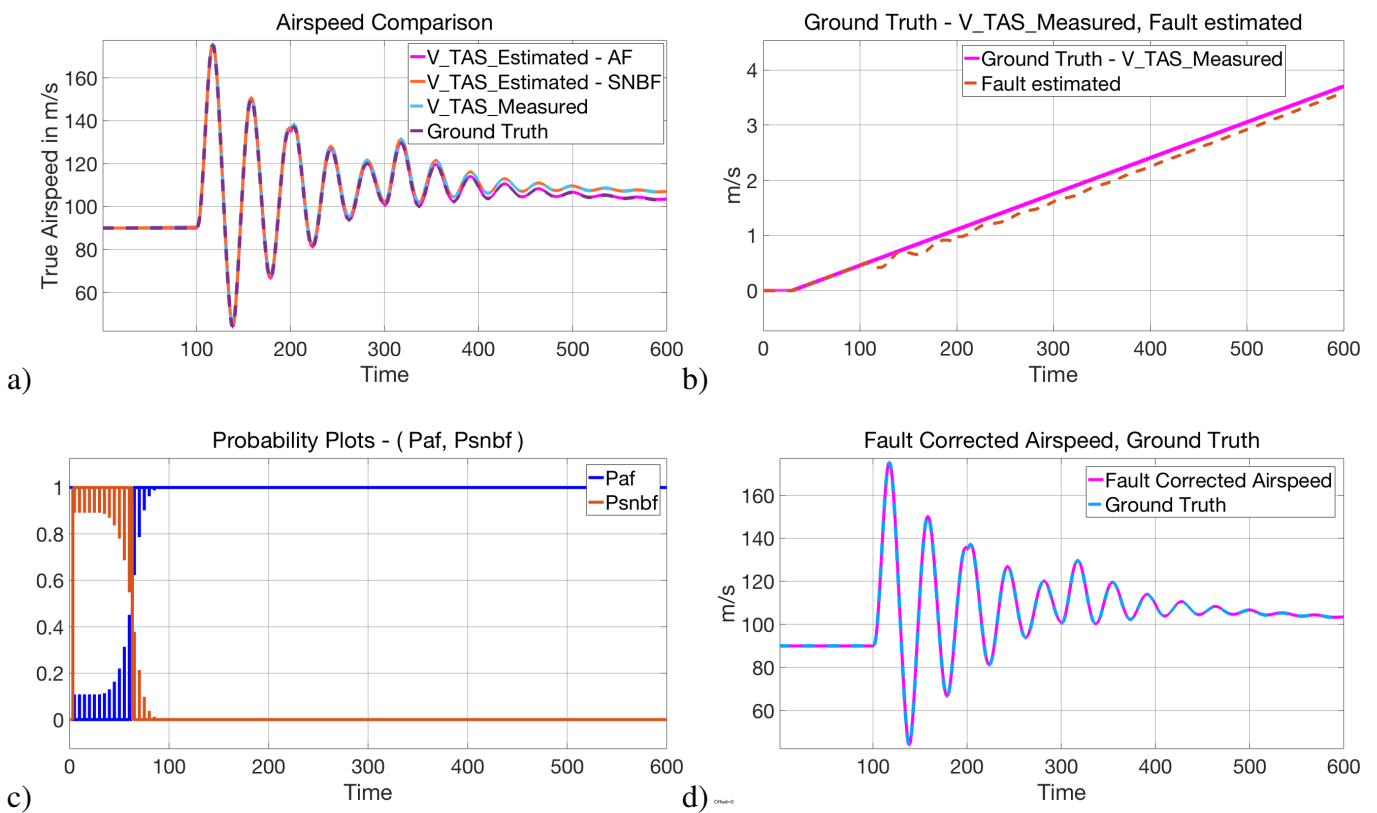

Fig. 9   ADS FDD performance to simulation with simple step fault. a) The airspeed comparison plot presents the airspeed data generated by both filters (SNBF & AF filter), alongside the fault-introduced airspeed and the ground truth airspeed. b) The plot represents the fault estimated by Augmented fault filter vs. fault introduced in the system. c) Represents the probability of the both the filters. d) Corrected Airspeed generated by augmented fault filter vs. ground speed.
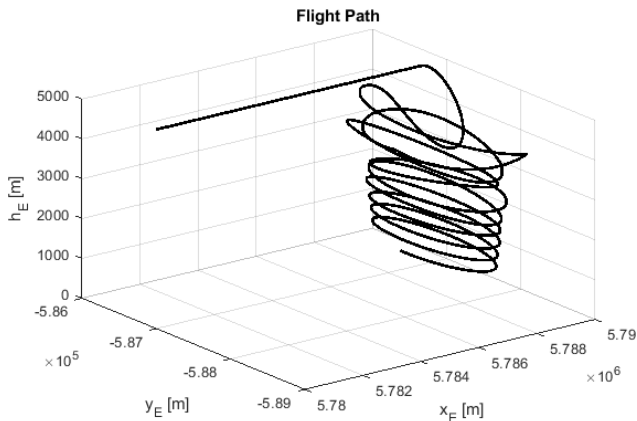
Fig. 10   Flight path - flight begins at 4000m with true airspeed 90m/s

13

Figure 10 represents the flight path of the simulated data used to test the fault detection algorithm.

Figure 11 shows the results of a ramp fault with a slope of $m = 0.0065$ which is a very gradual slope and which is triggered at 30 seconds. This test aims to simulate either the total pressure port-blocked scenario or the static pressure-blocked scenario. From Table 1 it is seen that when a single static port or all static ports are blocked, the airspeed indicator acts by decreasing during the climb and increasing during decent. It is seen from Figure 10 that the flight is descending and that a ramp fault introduction simulates the static port-block scenario. From table 1 it is seen that in the total pressure port blocked scenario the airspeed indicator acts as an altimeter, increasing during the climb and decreasing during the descent. This can be simulated by a negative slope to the measurement signal, as it is similar to the ramp fault signal and the figure 11 is convincing enough. An interesting observation is made here; it is seen at 30 s that the estimated fault follows the ramp, but the probability calculation indicates a fault only at 60 s. This happens because of the probability calculation dependency on the innovation and covariance of the filter, the innovation takes time to grow in a ramp fault scenario, especially when the ramp slope is small.

Fig. 11   ADS FDD performance to simulation with ramp fault to represent either total pressure port or static pressure port blocked. a) The airspeed comparison plot presents the airspeed data generated by both filters (SNBF & AF filter), alongside the fault-introduced airspeed and the ground truth airspeed. b) The plot represents the fault estimated by Augmented fault filter vs. fault introduced in the system. c) Represents the probability of both filters. d) Corrected Airspeed generated by augmented fault filter vs. ground speed.

Table 3   Results without measurement noise

Fault Scenario	Figure	Interpretation	Summary
Sample and Hold Both ports blocked	12	Probability Calculation suffers from high Innovation	Due to probability calculations failure The corrected airspeed has spikes
Ramp Fault - Either Static or Total Pressure port blocked	11	The FDD filter take extra 30 sec to identify the fault	The FDD filter perfectly Identifies Fault with some delay
Simple Step	9	The fault is accurately predicted	The FDD filter perfectly Identifies Fault
Pulse generator	8	The fault is accurately predicted	The FDD filter perfectly Identifies Fault

Table 4   Results with measurement noise

| Fault Scenario	Figure	Interpretation	Summary
Sample and Hold Both ports blocked	17	Probability Calculation suffers from measurement noise	Due to probability calculations failure The corrected airspeed has spikes
Ramp Fault - Either Static or Total Pressure port blocked	16	The FDD filter take extra 30 sec to identify the fault	The FDD filter perfectly Identifies Fault with some delay
Simple Step	15	The fault is accurately predicted	The FDD filter perfectly Identifies Fault
Pulse generator	14	The fault is accurately predicted	The FDD filter perfectly Identifies Fault

Figure 12 are the test plots with a sample and a hold fault introduced every 50 seconds and active for 50 seconds; these times are selected because it was noticed that if the fault is introduced at the start of simulation then the filter does not initialize correctly. From Table 1 it is seen that when both ports are blocked, the airspeed indicator remains constant despite the actual change in velocity even during maneuvers. The sample-and-hold faults simulate exactly this scenario as can be seen in figure 2.

a)

b)

c)

d)
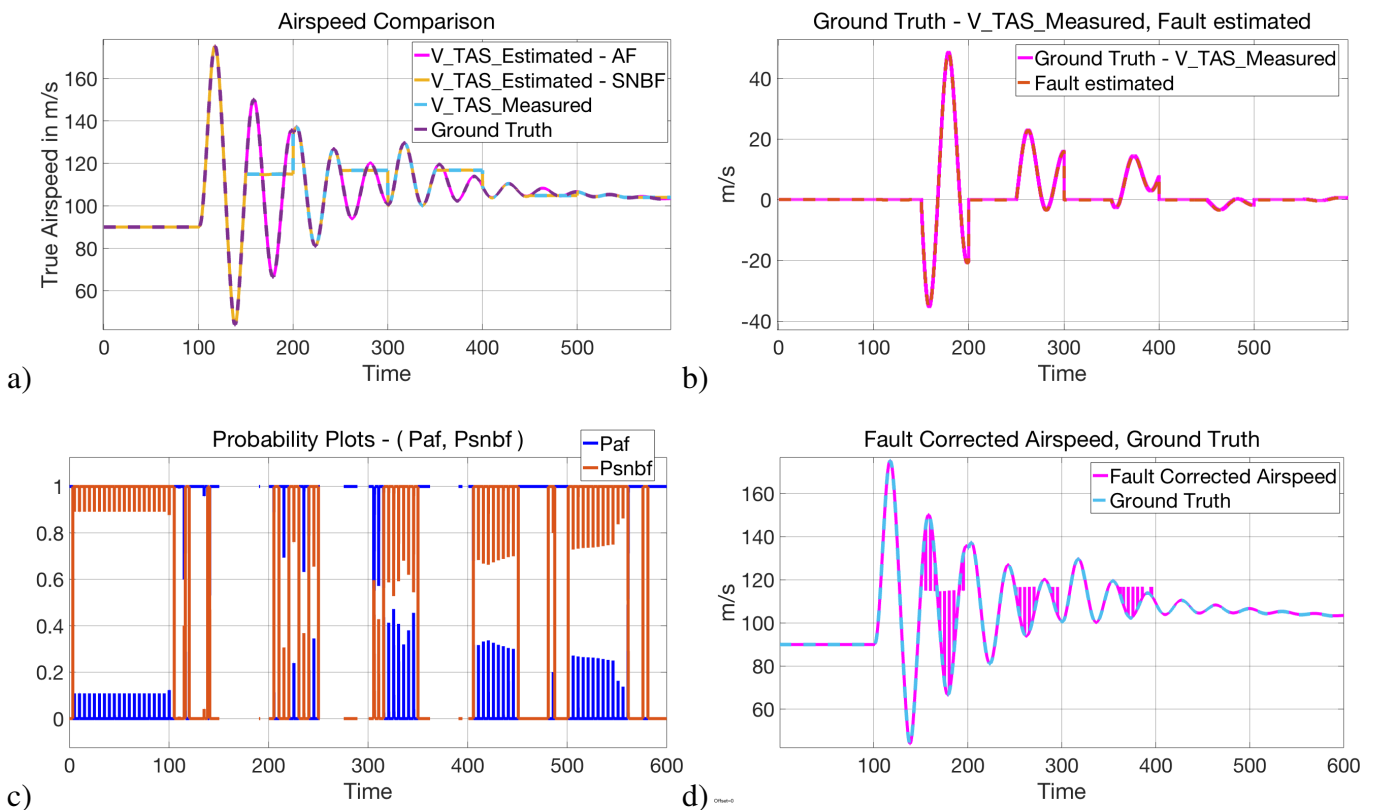
Fig. 12   ADS FDD performance to simulation with sample-and-hold fault to represent all ports blocked scenario. a) The airspeed comparison plot presents the airspeed data generated by both filters (SNBF & AF filter), alongside the fault-introduced airspeed and the ground truth airspeed. b) The plot represents the fault estimated by Augmented fault filter vs. fault introduced in the system. c) Represents the probability of the both filters. d) Corrected Airspeed generated by augmented fault filter vs. ground speed.

15

6.2 Results of the FDD algorithm with measurement noise

Testing FDD algorithms with measurement noise is essential to assess their effectiveness under real-world conditions. In this case, the FDD algorithm is evaluated by introducing band-limited white noise into the measurement signal (see Figure 13) that is a priori unknown to the filters.
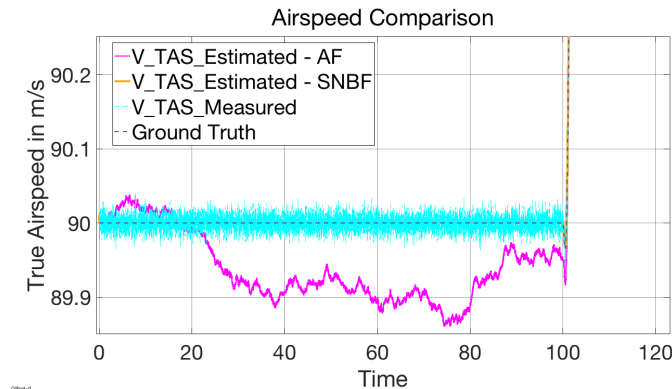

Fig. 13 **Measurement noise impact on estimation**

It can be seen from the figure 13 that for the augmented fault filter, the uncertainty in the measurement signal affects the estimation of the AF filter while it does not affect the sensor noise and bias filter. This is purely due to the fact that the fault estimated by the augmented fault filter is added as an additional state in the measurement function. Table 4 gives the summary of the results with measurement noise.

This subsection presents the robustness of the Fault Detection and Diagnosis (FDD) algorithm under the presence of measurement noise. Four test cases are discussed as seen in Table 4, each simulating faults through sample and hold, step, ramp, and pulse generator. The results are illustrated through four plots for each test case:

1) Probability of Correct Filter Selection: Showcasing the effectiveness of the Sensor Noise and Bias Filter (SNBF) and the Augmented Fault Filter (AF) algorithm in distinguishing the most appropriate filter.
2) Fault Estimation by AF Filter: Demonstrating the precision of the AF filter in estimating the fault.
3) Corrected Airspeed: Highlighting the capability of the proposed algorithm to generate a corrected airspeed despite the simulated faults.
4) Airspeed Comparison with Ground Truth: Validating the accuracy of the corrected airspeed against the actual airspeed data.

Figure 14 shows the results of the pulse fault injected into the noisy measurement. The estimated fault and the redundant airspeed are correlated as shown in Figure 8 with the measurement noise clearly visible on the estimated fault. Probability-based fault detection works despite having innovation uncertainty due to measurement noise provided the aircraft flies level. However, when the aircraft flies a high-amplitude maneuver the probability calculation fails due to a wide gap in the innovation between AF filter and SNBF filter. Despite probability calculation failure, a simple fault detection metric is used to obtain the redundant airspeed, and the airspeed remains valid throughout the simulation.
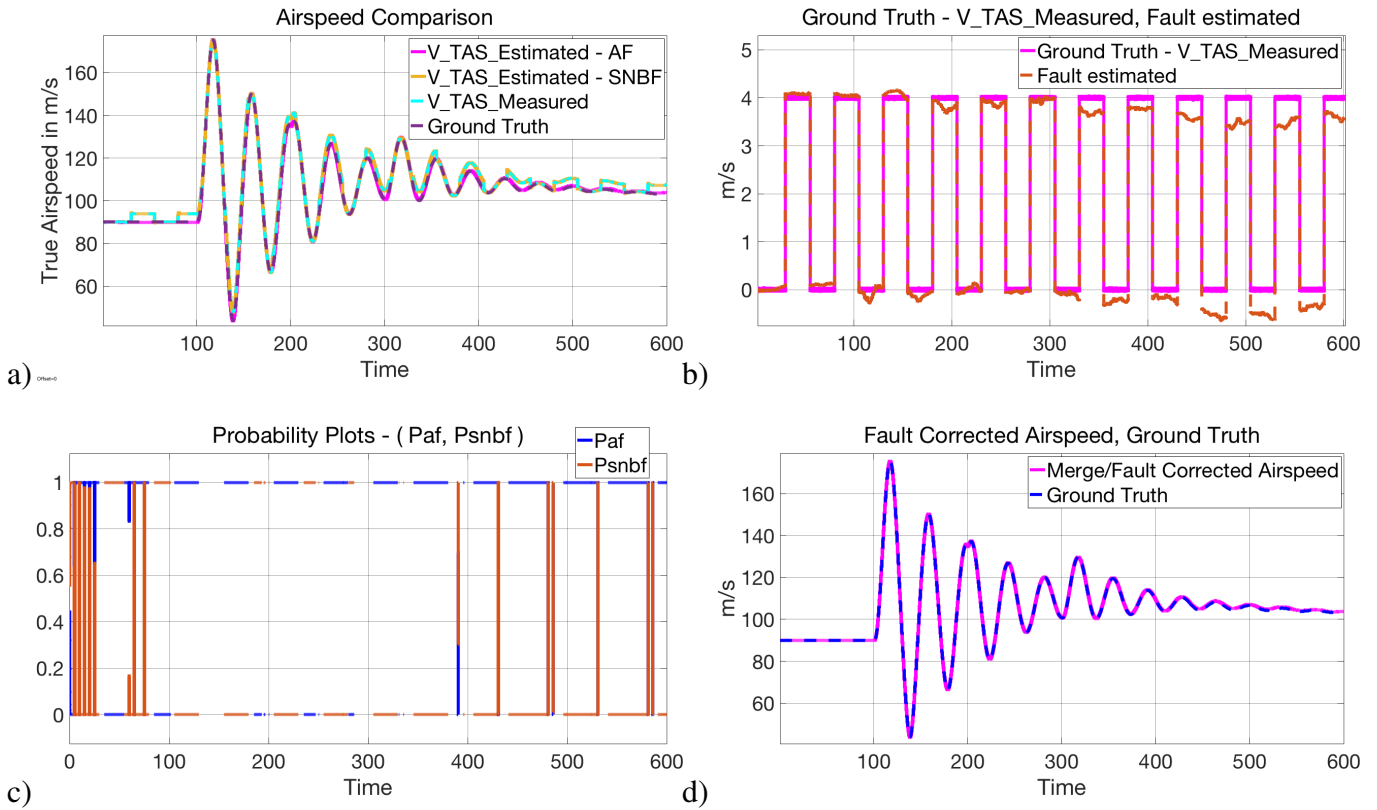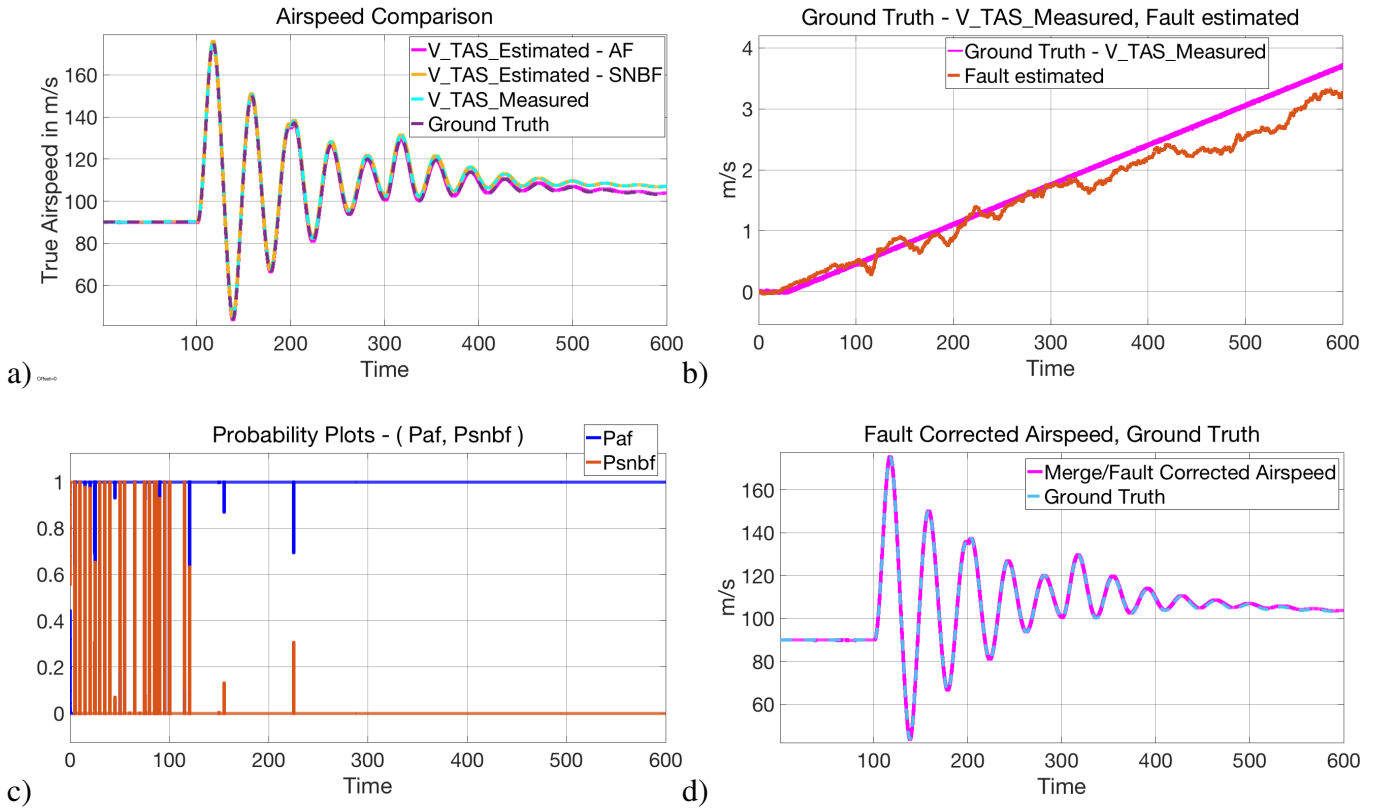

Fig. 14   ADS FDD performance to simulation with pulse generator fault - Measurement Noise. a) The airspeed comparison plot presents the airspeed data generated by both filters (SNBF & AF filter), alongside the fault-introduced airspeed and the ground truth airspeed. b) The plot represents the fault estimated by Augmented fault filter vs. fault introduced in the system. c) Represents the probability of the both filters. d) Corrected Airspeed generated by augmented fault filter vs. ground speed.

Figure 15 shows the simulation results for a step fault with measurement noise. When comparing the estimated fault between the figures with and without measurement noise (Figure 9), the effect of noise is observed in the estimated fault, since from 450 seconds the estimated trend of the fault seems to vary. The probability calculation suffers as observed before in Figure 14 the probability calculation seems stable until maneuvers are executed. However, it can be observed that many false alarms are raised, and the probability does not change when the fault is introduced. It is observed that when the filter is initiated the probability of the P_{SNBF} filter is 1 and P_{AF} is 0, but due to the uncertainty in the innovation of the AF filter, the combined probability shows that the AF filter has higher probability for the rest of the simulation. A clean probability change can be seen when a fault is introduced in 9 but not when measurement noise is introduced. The redundant airspeed estimation remains consistent with the ground truth.
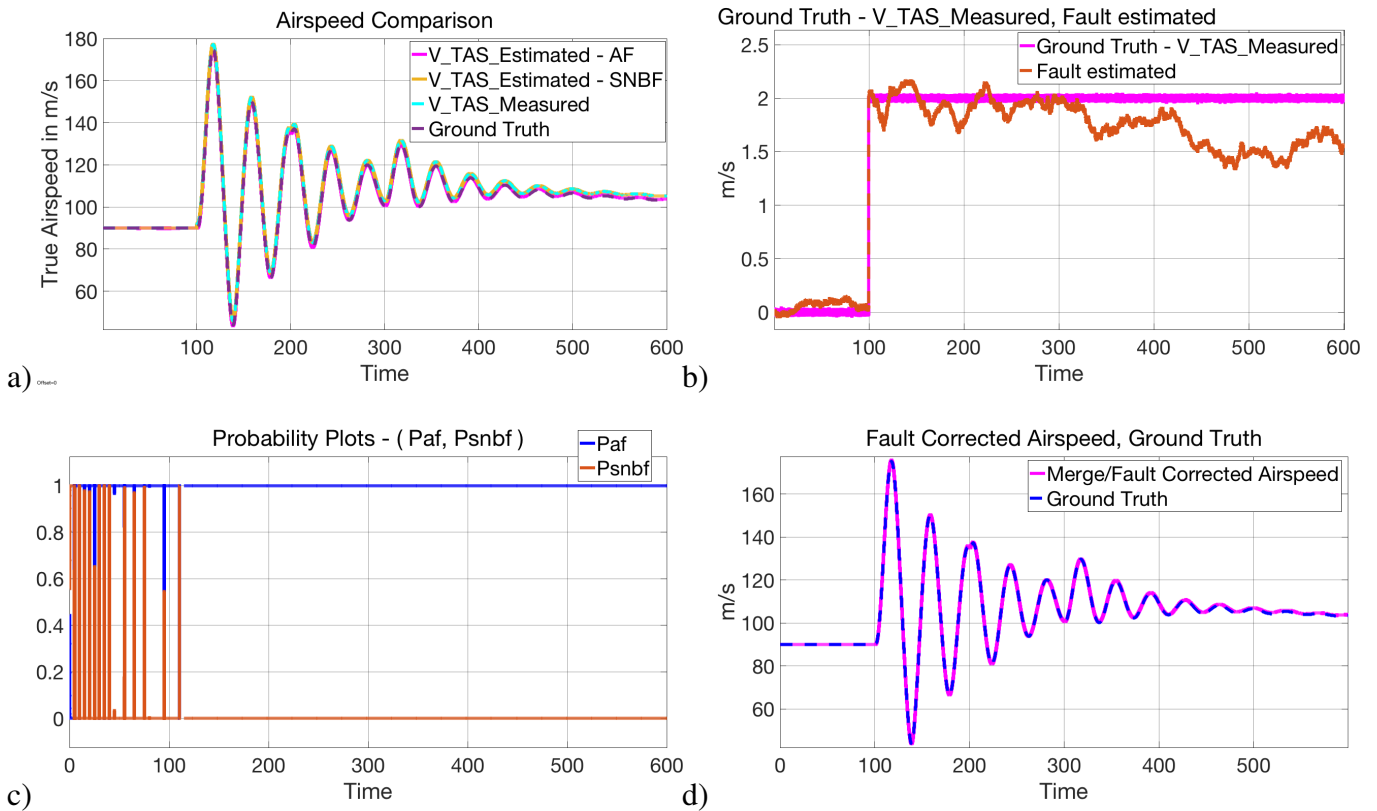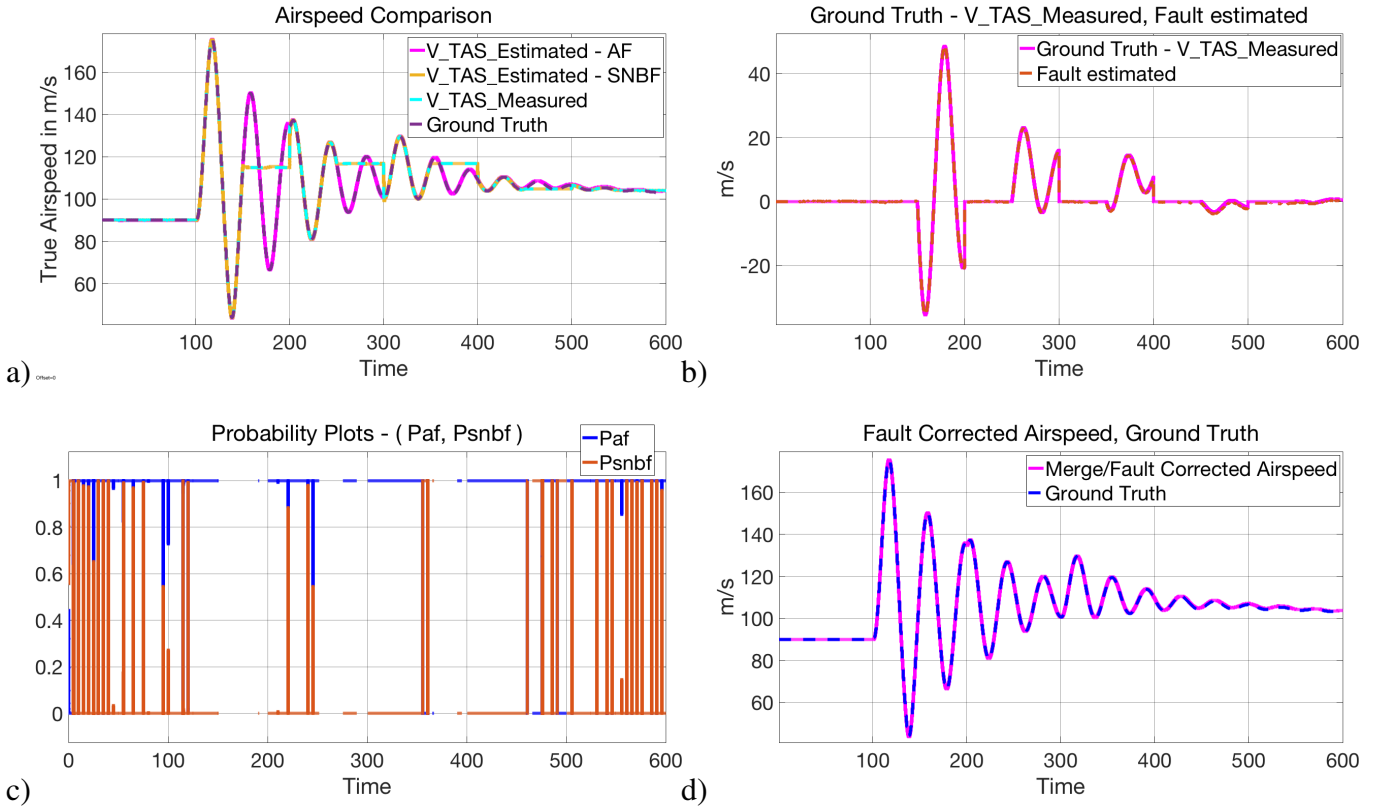

Fig. 15   ADS FDD performance to simulation with simple step fault - - Measurement Noise. a) The airspeed comparison plot presents the airspeed data generated by both filters (SNBF & AF filter), alongside the fault-introduced airspeed and the ground truth airspeed. b) The plot represents the fault estimated by Augmented fault filter vs. fault introduced in the system. c) Represents the probability of both filters. d) Corrected Airspeed generated by augmented fault filter vs. ground speed.

Figure 16 shows the simulation response graph to a ramp fault with slope $m = 0.0065$ and measurement noise, and the estimated fault follows the ground truth with minimal variance as can be seen from the fault estimated plot. Indeed, the probability are also in the expected trend. First, initializing with P_{SNBF} being the highest and then when the fault is introduced, P_{AF} is higher. Since these flight data have simulated measurement noise, the probability does not show the trend seen in the results without measurement noise, as seen in Figure 11.

Fig. 16   ADS FDD performance to simulation with ramp fault to represent either total pressure port or static pressure port blocked - Measurement Noise. a) The airspeed comparison plot presents the airspeed data generated by both filters (SNBF & AF filter), alongside the fault-introduced airspeed and the ground truth airspeed. b) The plot represents the fault estimated by Augmented fault filter vs. fault introduced in the system. c) Represents the probability of both filters. d) Corrected Airspeed generated by augmented fault filter vs. ground speed.

Figure 17 shows the FDD response to a sample-and-hold fault; from the estimated fault, the effects of noise cannot be clearly observed as the faults are correlated with the trend of airspeed when the faults are introduced. Since the variation in air speed is larger, variations in the estimated faults cannot be seen. The probability calculation for both types of fault fails for the reason stated above, but the redundant airspeed is consistent with ground truth.

Fig. 17 ADS FDD performance to simulation with sample-and-hold fault to represent all ports blocked scenario - Measurement Noise. a) The airspeed comparison plot presents the airspeed data generated by both filters (SNBF & AF filter), alongside the fault-introduced airspeed and the ground truth airspeed. b) The plot represents the fault estimated by Augmented fault filter vs. fault introduced in the system. c) Represents the probability of the both filters. d) Corrected Airspeed generated by augmented fault filter vs. ground speed.

7 Conclusion

In this paper, the detection and correction of reliable airspeed measurements due to various obstructions of the Pitot tube is studied. To improve airspeed estimation, an airspeed Fault Detection & Diagnosis (FDD) and redundant estimation routine based on the Double Model Adaptive Estimation (DMAE) principle is implemented and validated on simulation data. The filter performance is found to be not affected by the type of fault or the magnitude of the faults, but measurement noise affects the filter performance.

For the simulation with measurement noise, the probability calculations are not accurate because of uncertainty in measurement noise and also because innovation has great disparity. When probability calculations fail, the augmented fault (AF) filter states estimates are programmed to be assigned to the fault redundant airspeed. Therefore, we have the fault-augmented airspeed state at each time step. It

should be noted that probability calibrations fail in the case of noisy measurement signals when the vehicle is executing high-intensity maneuvers.

From the performance of the filter (Output Error Covariance and Root Mean Square Error), it can be seen that in the case with measurement signal noise, the estimation degrades after 400 seconds, but the filters performance stabilizes if run for a significant amount of time.

Refinement of probability calculations to work when measurement noise is introduced is a key area of future research.

Appendix

The covariance matrices of the SNBF filter is given in equation 14 and AF filters is given in equation 15 are constructed as follows:

$$
C_{SNBF} = \begin{bmatrix}
10e^{-10} & C_{V,\alpha} & C_{V,\beta} & C_{V,\phi} & C_{V,\theta} & C_{V,\psi} \\
C_{\alpha,V} & 10e^{-6} & C_{\alpha,\beta} & C_{\alpha,\phi} & C_{\alpha,\theta} & C_{\alpha,\psi} \\
C_{\beta,V} & C_{\beta,\alpha} & 10e^{-6} & C_{\beta,\phi} & C_{\beta,\theta} & C_{\beta,\psi} \\
C_{\phi,V} & C_{\phi,\alpha} & C_{\phi,\beta} & 3e^{-6} & C_{\phi,\theta} & C_{\phi,\psi} \\
C_{\theta,V} & C_{\theta,\alpha} & C_{\theta,\beta} & C_{\theta,\phi} & 3e^{-6} & C_{\theta,\psi} \\
C_{\psi,V} & C_{\psi,\alpha} & C_{\psi,\beta} & C_{\psi,\phi} & C_{\psi,\theta} & 3e^{-6}
\end{bmatrix}
\tag{14}
$$

$$
C_{AF} = \begin{bmatrix}
10e^{-10} & C_{V,\alpha} & C_{V,\beta} & C_{V,\phi} & C_{V,\theta} & C_{V,\psi} & C_{V,f_V} \\
C_{\alpha,V} & 10e^{-6} & C_{\alpha,\beta} & C_{\alpha,\phi} & C_{\alpha,\theta} & C_{\alpha,\psi} & C_{\alpha,f_V} \\
C_{\beta,V} & C_{\beta,\alpha} & 10e^{-6} & C_{\beta,\phi} & C_{\beta,\theta} & C_{\beta,\psi} & C_{\beta,f_V} \\
C_{\phi,V} & C_{\phi,\alpha} & C_{\phi,\beta} & 3e^{-6} & C_{\phi,\theta} & C_{\phi,\psi} & C_{\phi,f_V} \\
C_{\theta,V} & C_{\theta,\alpha} & C_{\theta,\beta} & C_{\theta,\phi} & 3e^{-6} & C_{\theta,\psi} & C_{\theta,f_V} \\
C_{\psi,V} & C_{\psi,\alpha} & C_{\psi,\beta} & C_{\psi,\phi} & C_{\psi,\theta} & 3e^{-6} & C_{\psi,f_V} \\
C_{fV,V} & C_{fV,\alpha} & C_{fV,\beta} & C_{fV,\phi} & C_{fV,\theta} & C_{fV,\psi} & 10e^{11}
\end{bmatrix}
\tag{15}
$$

References

[1] Fabio Balzano et al. "Air Data Sensor Fault Detection with an Augmented Floating Limiter". In: *International Journal of Aerospace Engineering* 2018 (Nov. 25, 2018). Ed. by Kenneth M. Sobel. Publisher: Hindawi, p. 1072056. ISSN: 1687-5966. DOI: 10.1155/2018/1072056. URL: https://doi.org/10.1155/2018/1072056.

[2] Derek Caveney. "Stochastic Path Prediction using the Unscented Transform with Numerical Integration". In: *2007 IEEE Intelligent Transportation Systems Conference*. 2007 IEEE Intelligent Transportation Systems Conference. Bellevue, WA, USA: IEEE, Sept. 2007, pp. 848–853. ISBN: 978-1-4244-1396-6. DOI: 10.1109/ITSC.2007.4357713. URL: http://ieeexplore.ieee.org/document/4357713/ (visited on 06/22/2023).

[3] Am Cho et al. "Airflow angle and wind estimation using GPS/INS navigation data and airspeed". In: *2013 13th International Conference on Control, Automation and Systems (ICCAS 2013)*. 2013 13th International Conference on Control, Automation and Systems (ICCAS 2013). ISSN: 2093-7121. Oct. 2013, pp. 1321–1324. DOI: 10.1109/ICCAS.2013.6704159.

[4] Mario L. Fravolini et al. "Data-Driven Schemes for Robust Fault Detection of Air Data System Sensors". In: *IEEE Transactions on Control Systems Technology* 27.1 (2019), pp. 234–248. DOI: `10.1109/TCST.2017.2758345`.

[5] Mario L. Fravolini et al. "Experimental interval models for the robust Fault Detection of Aircraft Air Data Sensors". In: *Control Engineering Practice* 78 (Sept. 2018), pp. 196–212. ISSN: 09670661. DOI: `10.1016/j.conengprac.2018.07.002`. URL: `https://linkinghub.elsevier.com/retrieve/pii/S0967066118302326` (visited on 05/09/2022).

[6] Paul Freeman, Peter Seiler, and Gary J. Balas. "Air data system fault modeling and detection". In: *Control Engineering Practice* 21.10 (2013), pp. 1290–1301. ISSN: 0967-0661. DOI: `https://doi.org/10.1016/j.conengprac.2013.05.007`. URL: `https://www.sciencedirect.com/science/article/pii/S0967066113000993`.

[7] Soren Hansen and Mogens Blanke. "Diagnosis of Airspeed Measurement Faults for Unmanned Aerial Vehicles". In: *IEEE Transactions on Aerospace and Electronic Systems* 50.1 (Jan. 2014), pp. 224–239. ISSN: 0018-9251. DOI: `10.1109/TAES.2013.120420`. URL: `http://ieeexplore.ieee.org/document/6809912/` (visited on 07/25/2022).

[8] Tor A. Johansen et al. "On estimation of wind velocity, angle-of-attack and sideslip angle of small UAVs using standard sensors". In: *2015 International Conference on Unmanned Aircraft Systems (ICUAS)*. 2015 International Conference on Unmanned Aircraft Systems (ICUAS). June 2015, pp. 510–519. DOI: `10.1109/ICUAS.2015.7152330`.

[9] F. Adhika Pradipta Lie and Demoz Gebre-Egziabher. "Synthetic Air Data System". In: *Journal of Aircraft* 50.4 (2013). _eprint: https://doi.org/10.2514/1.C032177, pp. 1234–1249. DOI: `10.2514/1.C032177`. URL: `https://doi.org/10.2514/1.C032177`.

[10] P. Lu. "Fault Diagnosis and Fault-Tolerant Control for Aircraft Subjected to Sensor and Actuator Faults". PhD thesis. Delft University of Technology, 2016. DOI: `10.4233/UUID:11BE69D2-44AE-429C-9746-7E3CED35F464`. URL: `http://resolver.tudelft.nl/uuid:11be69d2-44ae-429c-9746-7e3ced35f464` (visited on 07/04/2022).

[11] Peng Lu et al. "Air Data Sensor Fault Detection and Diagnosis in the Presence of Atmospheric Turbulence: Theory and Experimental Validation With Real Flight Data". In: *IEEE Transactions on Control Systems Technology* PP (Oct. 2020). DOI: `10.1109/TCST.2020.3025725`.

[12] Peng Lu et al. "Double-model adaptive fault detection and diagnosis applied to real flight data". In: *Control Engineering Practice* 36 (Mar. 2015), pp. 39–57. ISSN: 09670661. DOI: `10.1016/j.conengprac.2014.12.007`. URL: `https://linkinghub.elsevier.com/retrieve/pii/S0967066114002809` (visited on 07/18/2022).

[13] Peng Lu et al. "Nonlinear aircraft sensor fault reconstruction in the presence of disturbances validated by real flight data". In: *Control Engineering Practice* 49 (2016), pp. 112–128. ISSN: 0967-0661. DOI: `https://doi.org/10.1016/j.conengprac.2016.01.012`. URL: `https://www.sciencedirect.com/science/article/pii/S0967066116300120`.

[14] M.D.W. McIntyre and C.A. Gossett. "The Boeing 777 Fault Tolerant Air Data and Inertial Reference System-a new venture in working together". In: *Proceedings of 14th Digital Avionics Systems Conference*. Nov. 1995, pp. 178–183. DOI: `10.1109/DASC.1995.482827`.

[15] Dubravko Miljković. "Fault Detection Methods - A Literature Survey". In: (), p. 6.

[16] Matthew B. Rhudy et al. "Aircraft model-independent airspeed estimation without pitot tube measurements". In: *IEEE Transactions on Aerospace and Electronic Systems* 51.3 (July 2015). Conference Name: IEEE Transactions on Aerospace and Electronic Systems, pp. 1980–1995. ISSN: 1557-9603. DOI: `10.1109/TAES.2015.130631`.

[17] L. Van Eykeren and Q.P. Chu. "Sensor fault detection and isolation for aircraft control systems by kinematic relations". In: *Control Engineering Practice* 31 (Oct. 2014), pp. 200–210. ISSN: 09670661. DOI: `10.1016/j.conengprac.2014.02.017`. URL: `https://linkinghub.elsevier.com/retrieve/pii/S0967066114000884` (visited on 05/02/2022).

[18] Wonkeun Youn et al. "Aerodynamic Model-Aided Estimation of Attitude, 3-D Wind, Airspeed, AOA, and SSA for High-Altitude Long-Endurance UAV". In: *IEEE Transactions on Aerospace and Electronic Systems* 56.6 (2020), pp. 4300–4314. DOI: 10.1109/TAES.2020.2988962.

[19] Wonkeun Youn et al. "Model-Aided Synthetic Airspeed Estimation of UAVs for Analytical Redundancy". In: *IEEE Robotics and Automation Letters* 6.3 (July 2021). Conference Name: IEEE Robotics and Automation Letters, pp. 5841–5848. ISSN: 2377-3766. DOI: 10.1109/LRA.2021.3086428.

[20] Yunmei Zhao et al. "Robust Data-Driven Fault Detection: An Application to Aircraft Air Data Sensors". In: *International Journal of Aerospace Engineering* 2022 (Mar. 16, 2022). Ed. by Guillermo Valencia-Palomo. Publisher: Hindawi, p. 2918458. ISSN: 1687-5966. DOI: 10.1155/2022/2918458. URL: https://doi.org/10.1155/2022/2918458.

23